

Electrocatalytic dechlorination of 2,4-dichlorophenoxyacetic acid using nanosized titanium nitride doped palladium/nickel foam electrodes in aqueous solutions



Chen Sun, Shams Ali Baig, Zimo Lou, Jin Zhu, Zhuoxing Wang, Xia Li, Jiahua Wu, Yifu Zhang, Xinhua Xu*

Department of Environmental Engineering, Zhejiang University, Hangzhou 310058, People's Republic of China

ARTICLE INFO

Article history:

Received 17 December 2013
Received in revised form 4 March 2014
Accepted 3 April 2014
Available online 13 April 2014

Keywords:

2,4-D
Adsorption theory
Electrocatalytic dechlorination
nTiN doped Pd/Ni foam electrode
Reduction mechanism

ABSTRACT

Nanosized titanium nitride (nTiN) doped palladium/nickel (Pd/Ni) foam electrodes were successfully prepared via electroless deposition method. The electrodes were evaluated by different techniques including field emission scanning electron microscopy (FE-SEM), transmission electron microscopy (TEM), X-ray photoelectron spectroscopy (XPS), X-ray diffraction (XRD) and linear sweep voltammetry (LSV). FE-SEM images demonstrated that two different morphologies existed in the Pd layer after nTiN doping. The nTiN doped Pd/Ni foam electrodes were found to be highly effective for electrochemical reductive dechlorination of 2,4-dichlorophenoxyacetic acid (2,4-D) with excellent activity and stability, as revealed by batch experiments. Under the conditions of nTiN doping content of 2 mg, Pd loading of 0.44 mg cm^{-2} , the energetic electrode achieved nearly 100% removal of 2,4-D ($0.226 \text{ mmol L}^{-1}$) within 2 h at a current density of 1.667 mA cm^{-2} . However, the removal efficiency reached only 57.13% when a normal Pd/Ni foam electrode with identical Pd loading and current density was utilized. A successive 2,4-D reductive dechlorination process was observed. *o*-Chlorophenoxyacetic acid (*o*-CPA), *p*-chlorophenoxyacetic acid (*p*-CPA) and phenoxyacetic acid (PA) were detected and identified as transformation products. Regression analysis proved that the pseudo-first order kinetic model was not suitable to describe the dechlorination process on nTiN doped Pd/Ni foam electrodes due to the appearance of a plateau in the beginning of the curve. Moreover, an adsorption theory for Pd chemisorption of active hydrogen atom was proposed to better explain the phenomenon. An adsorption equilibrium of hydrogen existed in the Pd lattice between hydrogen in Pd solid solution and hydrogen in metal hydride, which would influence the effective utilization of active hydrogen atom [H] for dechlorination treatment. An indirect reduction mechanism of the 2,4-D dechlorination on the as-prepared electrodes was also elucidated.

© 2014 Elsevier B.V. All rights reserved.

1. Introduction

2,4-D is a herbicidally active member of the chlorophenoxyalkanoic acid series, which is known as chlorinated organic compounds (COCs). It is an effective systemic herbicide to control many types of broadleaf weeds and pests in agricultural fields worldwide [1–4]. However, in recent years the contamination of 2,4-D in the environment has raised enormous concerns due to its high solubility [5], poor biodegradability [6], toxicological effects on aquatic organisms and public health [7,8]. Furthermore, the World Health Organization (WHO) defined 2,4-D as moderately toxic and

recommended its maximum allowable concentration of $100 \mu\text{g L}^{-1}$ in drinking water [9]. Therefore, effective remediation techniques for 2,4-D detoxification are highly sought after.

The presence of chlorine atom in COCs structure is considered to be the main cause of its toxic properties [10]. Thus, the development of reductive dechlorination treatment has been triggered. In this treatment process, with the whole carbon skeletons remaining intact, chlorine atoms are selectively removed and replaced by hydrogen. Application of zero-valent iron nanoparticles (nZVI) has been regarded as an effective dechlorination technology for the removal of COCs [11]. Nonetheless, nano size and high surface reactivity characteristics of iron nanoparticles lead to the problems of easy agglomeration and surface passivation, which have been a major bottleneck for the large scale application of nZVI and its derivative technologies [12,13]. Biological reductive dechlorination

* Corresponding author. Tel.: +86 571 88982031; fax: +86 571 88982031.
E-mail address: xuxinhua@zju.edu.cn (X. Xu).

technology has also been reported in literature as an innovative method for COCs treatment [14,15]. But this approach was shown to be quite tedious and effective only for the treatment of less chlorinated congeners [16,17].

Recently, electrochemical reductive treatment has been recognized as a promising approach for COCs dechlorination due to its unique characteristics such as rapid reaction rate, low apparatus cost, mild reaction conditions and the absence of recalcitrant secondary contaminants [18]. Compared with other available options, electrochemical reductive treatment is supported by more robust and enduring source of electron and hydrogen. Several studies have been reported on the electrochemical reductive treatment. For example, Yang et al. [19] achieved high efficiency conversion of 4-chlorobiphenyl to biphenyl in an electrochemical dechlorination process. Similarly, Xie et al. [20] reported the efficient and quantitative transformation of trichloroethylene to ethane. Cathode materials are considered the most critical parameter during the electrochemical reductive process due to its predominant influence on reaction pathway and treatment efficiency [21]. The cathode substrates and the catalytically active materials loaded on the substrates are the two essential parts for the dechlorination cathodes. Numerous materials have been utilized as cathode substrates including carbon materials (activated carbon cloths, activated carbon fibers) [22], metal materials (Platinum, Copper) [23] and conducting polymers (polypyrrole, polyaniline) [24]. Recently, Ni foam, a commercial material with high electrical conductivity, good mechanical strength and desirable three dimensional (3D) structures, has been applied in electrochemical field, such as electrochemical capacitors [25], fuel cells [26] and lithium ion batteries [27]. As compared to other conventional two dimensional (2D) flat structures, Ni foam provides more sufficient reactive sites due to its large specific surface area. Catalytically active materials loading on the cathode substrates for high dechlorination attract more attention these days. Noble metals such as Pd, Pt, Ru and Rh have been reported to possess excellent properties to facilitate electrocatalytic dechlorination. Among them, Pd was found to be more effective due to its superior ability to absorb hydrogen into lattice and to further form active atomic hydrogen [H] for effective dechlorination of COCs [28]. Extensive efforts have been made to enhance the catalytic efficiency of Pd by adding middle layers of metals in group IB of the periodic table [29] and conducting polymers [24]. Nevertheless, to the best of our knowledge, modification inside the Pd layer has not yet been investigated in detail, which presumably could enhance its electrocatalytic activity by changing the surface morphology and the internal electrical property.

In this study, nanosized titanium nitride (nTiN) was employed as a good candidate of material for modification of Pd layer owing to its fascinating features including chemical stability [30], low electric resistivity [31] and attractive catalytic abilities [32]. TiN has been employed as a cathode [33], whereby the researchers used nTiN loaded cathode for the effective debromination of 2,2',4,4'-tetrabromodiphenyl ethers. Based on the reliable TiN electrochemical performance, it is rational to hypothesize that the conventional catalyst Pd modified by nTiN can show better catalytic performance toward electrochemical reductive dechlorination. Herein, we reported, for the first time, the synthesis of nTiN doped Pd/Ni foam electrodes. The electrocatalytic dechlorination performance of nTiN doped Pd/Ni foam electrode was compared with normal Pd/Ni foam electrode in a two-compartment electrochemical system. The effects of nTiN doping content and Pd loading on dechlorination efficiency were also investigated. The catalytic mechanism for Pd on dechlorination reaction was derived. Moreover, the mechanism of 2,4-D dechlorination on nTiN doped Pd/Ni electrode was ultimately elucidated.

2. Experimental

2.1. Materials and reagents

Nickel foam (pore density, 100 ppi; S_{BET} , $1.2 \text{ m}^2 \text{ g}^{-1}$) used as the electrode substrates was provided by Shenzhen Rolinsia Power Materials Ltd., China. Palladium chloride (PdCl_2 ; $\geq 99.97\%$) was purchased from the Sinopharm Chemical Reagent Co., Ltd., China. Nanosized titanium nitride (nTiN; $\geq 99.9\%$) was from Aladdin Reagent Inc., China. 2,4-Dichlorophenoxyacetic acid (2,4-D; $\geq 97\%$), *p*-chlorophenoxyacetic acid (*p*-CPA; $\geq 98\%$) and phenoxyacetic acid (PA; $\geq 98\%$) were provided by Jingchun Reagent Co. Ltd., Shanghai. *o*-Chlorophenoxyacetic acid (*o*-CPA; $\geq 98\%$) was purchased from Alfa Aesar Chemical Co. Ltd., Tianjin. A 2,4-D stock solution was prepared by dissolving 5 g of 2,4-D in 1 L methanol and stored at 4°C before use. All the chemicals were of analytical grade and used as received without further purification. Deionized water (with a specific conductivity $\geq 18.2 \text{ m}\Omega \text{ cm}^{-1}$) obtained from a Millipore Milli-Q system was used throughout the experiments.

2.2. Electrode preparation

nTiN doped Pd/Ni foam electrodes were prepared as per specifications. Prior to the preparation, Ni foam substrates ($20 \text{ mm} \times 30 \text{ mm} \times 1.2 \text{ mm}$) were degreased in acetone for 20 min with ultrasonic agitation and subsequently immersed in 80 g L^{-1} sulfuric acid for 5 min to remove the oxidized layer, followed by a thorough rinse with deionized water. Then, nTiN doped Pd/Ni foam electrodes were prepared using an electroless deposition method. Firstly, PdCl_2 and NaCl with a molar ratio of 1:3 were added into a conical flask (100 mL) in order to increase the solubility by forming complex $[\text{PdCl}_4]^{2-}$. Secondly, a certain amount of stable nTiN suspension was prepared by dispersing nTiN powder in the conical flask containing PdCl_2 and NaCl via sonication for 0.5 h. Thirdly, the pretreated Ni foam substrates were immersed at the bottom of the conical flask. Lastly, the conical flask was allowed to stand for 12 h with vigorous shaking at a temperature of 32°C . The electrodes with different Pd loadings and nTiN doping contents were prepared by varying the dosage of certain reagents in the reaction solution.

The Pd/Ni foam electrode as a control for comparison was prepared according to previously published procedure [34].

2.3. Batch experiments

All batch experiments for the electrochemical dechlorination of 2,4-D were performed in a two-compartment electrolytic cell inside a temperature-controlled bath ($25 \pm 0.1^\circ\text{C}$). The anode and cathode cells with a volume capacity of 50 mL and 100 mL, respectively, were separated by a cation-exchange membrane Nafion-117 that prevented chloride ion from generating Cl_2 on anode. For each trial, 40 mL and 80 mL of 10 mmol L^{-1} Na_2SO_4 solutions were transferred into anode and cathode cell, respectively. 0.8 mL of the 5 g L^{-1} 2,4-D stock solution was added into the cathode cell to achieve an initial concentration of 50 mg L^{-1} . nTiN doped Pd/Ni foam electrode or Pd/Ni foam electrode and platinum foil ($20 \text{ mm} \times 30 \text{ mm}$) worked as cathode and anode, respectively. The anode and cathode were positioned vertically and parallel to each other with an approximate distance of 80 mm. A certain constant current was supplied by an SK1760SL20A direct-current regulated power supply and determined accurately by a multimeter device. Homogeneous phase in the cathode cell was attained by constant magnetic stirring. Aliquots of samples (0.8 mL) were withdrawn from the cathode cell for further analysis at pre-determined time intervals.

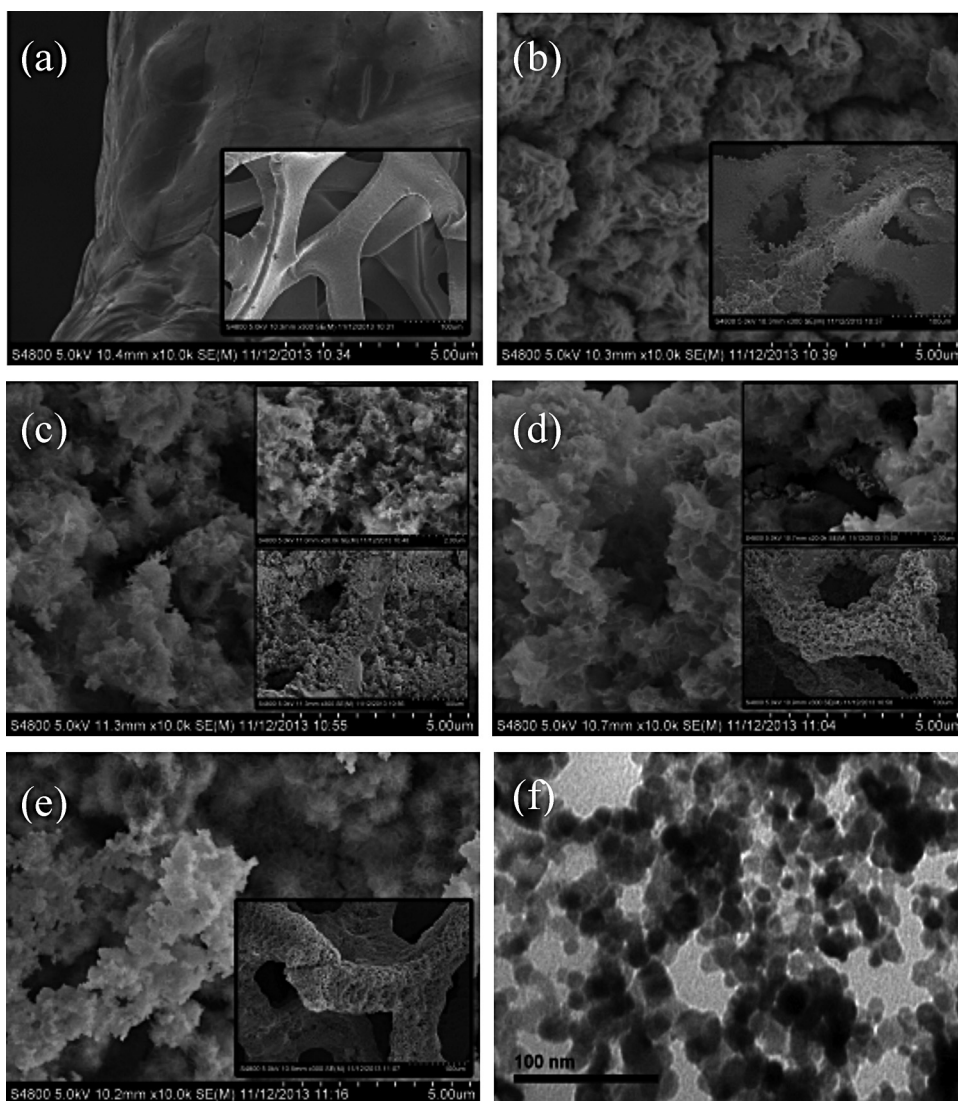


Fig. 1. FE-SEM images of (a) Ni foam electrode, (b) Pd/Ni foam electrode (Pd loading = 0.44 mg cm^{-2}), (c) nTiN doped Pd/Ni foam electrode (Pd loading = 0.44 mg cm^{-2} , nTiN doping content = 2 mg (for the whole electrode)), (d) nTiN doped Pd/Ni foam electrode after dechlorination reaction (Pd loading = 0.44 mg cm^{-2} , nTiN doping content = 2 mg), (e) nTiN doped Pd/Ni foam electrode (Pd loading = 0.44 mg cm^{-2} , nTiN doping content = 4 mg) and (f) TEM image of nTiN.

2.4. Analytical methods and electrode characterization

The concentrations of 2,4-D, *o*-CPA, *p*-CPA and PA were determined with a SHI-MADZU high-performance liquid chromatography at 283 nm with an Agilent TC-C18 column (150×4.6). The mobile phase was a 60:40 (v/v) mixture of methanol: 0.2% H_3PO_4 (in water), and 0.5 mL min^{-1} flow rate was maintained. The injected sample volume was $20 \mu\text{L}$.

The conversion of 2,4-D was calculated as the ratio between the amount of 2,4-D being consumed and the initial concentration of 2,4-D in cathode cells. The yield of PA was determined as the molar ratio between the amount of PA being generated and initial concentration of 2,4-D. The average current efficiency was calculated as described earlier [34].

The surface morphology of the electrodes was examined by a Hitachi S-4800 cold field emission scanning electron microscope (FE-SEM). Transmission electron microscopy (TEM) images of nTiN particles were obtained by a JEOL JEM-1200EX electron microscope. X-ray diffraction (XRD) analysis was performed to identify the phase structure, using a PANalytical X' Pert PRO X-ray diffractometer machine with $\text{Cu K}\alpha$ radiation, operating at 40 kV and 40 mA with a scan step size of 0.0167° and time per step of 10.16 s.

X-ray photoelectron spectroscopy (XPS) analysis was performed with a Thermo Fisher Escalab 250Xi X-ray photoelectron spectrometer. Linear sweep voltammetry (LSV) of electrodes was scanned in $10 \text{ mmol L}^{-1} \text{ Na}_2\text{SO}_4$ solution on a CHI604Cs650D (Shanghai Chenhua, China) electrochemical workstation, using a three-electrode system inside an undivided electrolytic cell with a scan rate of 20 mV s^{-1} . The working electrode ($20 \text{ mm} \times 30 \text{ mm}$) is individual electrodes under study, the counter electrode ($20 \text{ mm} \times 30 \text{ mm}$) was a platinum foil, and the reference electrode was a saturated Ag/AgCl electrode. The working and counter electrode were parallel to each other with the distance of 20 mm, and the reference electrode was placed in Luggin capillary near the working electrode. The potential of the saturated Ag/AgCl electrode was 0.199 V compared to that of a standard hydrogen electrode (SHE) at 298 K.

3. Results and discussion

3.1. Electrode characterization

Fig. 1 shows FE-SEM images of Ni, Pd/Ni, freshly-prepared and used nTiN doped Pd/Ni foam electrodes and nTiN doped Pd/Ni foam electrodes with higher nTiN doping content. The bare Ni foam

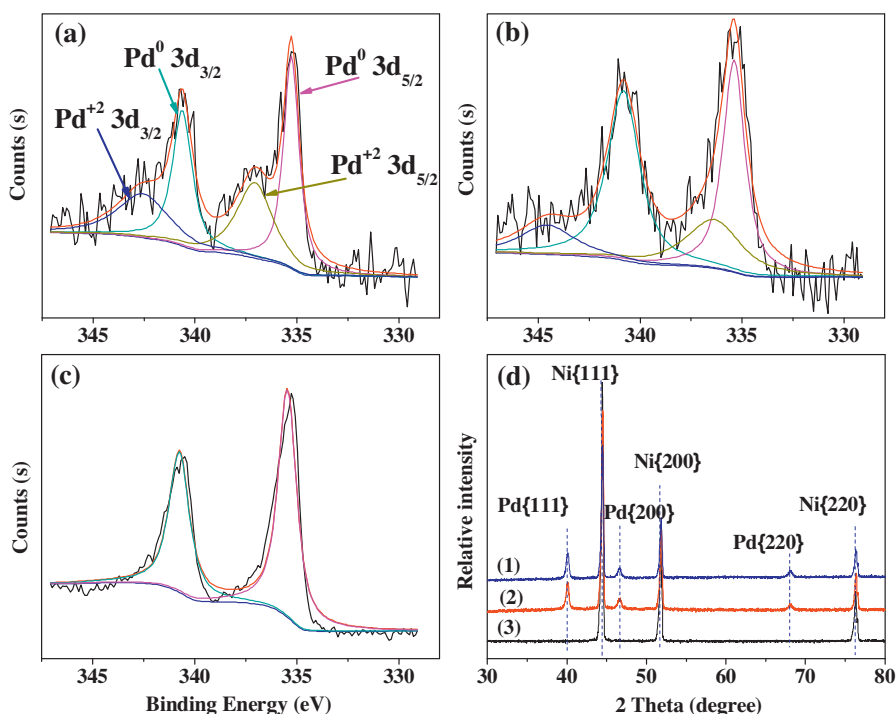


Fig. 2. XPS of Pd 3d spectra on (a) Pd/Ni foam electrode, (b) nTiN doped Pd/Ni foam electrode, (c) nTiN doped Pd/Ni foam electrode after dechlorination reaction and (d) XRD patterns of (1) nTiN doped Pd/Ni foam electrode (Pd loading = 1.78 mg cm^{-2} , nTiN doping content = 2 mg), (2) Pd/Ni foam electrode (Pd loading = 1.78 mg cm^{-2}), (3) nTiN doped Pd/Ni foam electrode (Pd loading = 0.44 mg cm^{-2} , nTiN doping content = 2 mg).

exhibited its typical scaffold architecture and the surface was relatively smooth with some depressions (Fig. 1a). It was apparent that the Pd layer has been successfully deposited on the Pd/Ni foam electrode (Fig. 1b), and the granular structure appeared on the surface with some cluster crystal on the layer edges. At a higher magnification, dense regular protuberances surrounded by cracks could be clearly identified. In contrast, after the nTiN doping, the electrode surface became more chaotic (Fig. 1c), which resulted in a high specific surface area. The regular protuberances were replaced by the large scale silk-like flaky wrinkle structures on the nTiN doped Pd/Ni foam electrode. Meanwhile, small nTiN particles were found to be attached to the flaky body. After the dechlorination reaction (Fig. 1d), the amount of nTiN reduced suggesting that nTiN on the flake suffered from a desquamation problem. It was interesting to note that a gap of the flaky wrinkle structure appeared on the used nTiN doped Pd/Ni foam electrode. As a result, the protuberances structure observed on Pd/Ni foam electrodes was visible again and some nTiN particles were on the margin illustrating that the protuberance was actually covered by the flaky wrinkle structure. Therefore, two morphologies could co-exist in the Pd layer after the doping of nTiN. When more nTiN was doped into the electrode, the flaky wrinkle structure disappeared, as shown in Fig. 1e. The nTiN agglomerated together and directly covered the protuberances. Moreover, the nTiN size was found to be around 20 nm, as revealed by TEM image (Fig. 1f).

In order to investigate the valence state of Pd on the electrodes, typical XPS survey spectra of Pd 3d were obtained for Pd/Ni foam electrode and nTiN doped Pd/Ni foam electrodes before and after the 2,4-D dechlorination reaction. Based on the peak fitting analysis presented in Fig. 2a–c, both the Pd 3d spectrum on the Pd/Ni foam and fresh nTiN doped Pd/Ni foam electrode were found to exhibit two pairs of spin–orbit components. However, only the major pair appeared on the used nTiN doped Pd/Ni foam electrode. The major spin–orbit component pair corresponding to Pd $3d_{5/2}$ and Pd $3d_{3/2}$ suggested that the Pd layer was predominated by the metallic palladium Pd⁰. The binding energies of the major

spin–orbit split doublet on the Pd/Ni foam electrode were 335.3 eV and 340.6 eV, respectively. However, they were located at 335.5 eV and 340.8 eV on nTiN doped electrodes before and after the dechlorination, a positive shift by 0.2 eV compared to that of a Pd/Ni foam electrode. The shift was probably due to the interaction between Pd particles and nTiN, which was previously confirmed by Thotiyl et al. [35]. The minor spin–orbit component pair at higher binding energy illustrated the presence of Pd with lower electron density Pd⁺², which could be assigned to PdO and PdO_{ads} species during the electrode preparation [36]. Meanwhile, Li et al. [37] confirmed that this minor pair could be attributed to the formation of transitional Pd–Cl bond during dechlorination process. In our experiment additional NaCl was added during the preparation process in order to better dissolve the PdCl₂, it could be speculated that Pd–Cl bond was subsequently formed by the excess Cl[−] present in the solution. After the dechlorination reaction minor spin–orbit component pair disappeared, which probably resulted from the current reduction effect on Pd. Consequently, the cathodic polarization could inhibit the catalyst deactivation that resulted from Pd oxidation or chloride adsorption.

XRD was utilized as an effective method for phase identification. Fig. 2d shows the XRD patterns of electrodes with different nTiN doping contents and Pd loadings for 2θ diffraction angles ranging from 30° to 80°. Notably, all the three patterns showed typical diffraction peaks at 44.5°, 51.8° and 76.2°, corresponding to the (1 1 1), (2 0 0) and (2 2 0) planes of metal Ni, respectively (JCPDS File No. 04-0850). When Pd loading was 1.78 mg cm^{-2} , the XRD patterns of electrodes with and without nTiN doping (Fig. 2d(1, 2)) exhibited little difference. The diffraction peaks at 40.1°, 46.7° and 68.1° could be attributed to (1 1 1), (2 0 0) and (2 2 0) planes of Pd, respectively (JCPDS File No. 65-2867) indicating the successful deposition of crystal lattice Pd on the Ni foam. But there was no nTiN peak appeared. As shown in Fig. 2d(3), when Pd loading was reduced to 0.44 mg cm^{-2} , the Pd typical peaks disappeared. Thus, nTiN could not be detected by XRD possibly due to the low content.

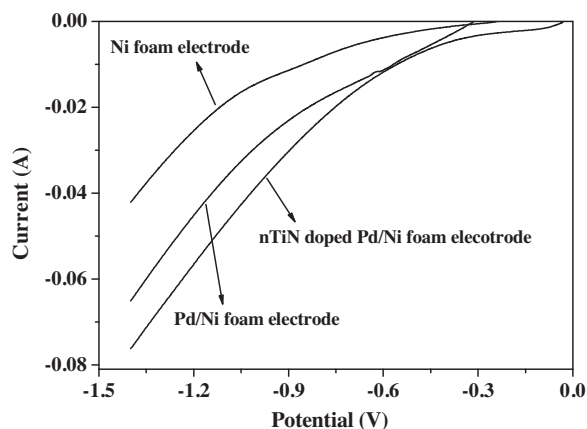


Fig. 3. Linear sweep voltammetry curves of Ni foam, Pd/Ni foam and nTiN doped Pd/Ni foam electrode.

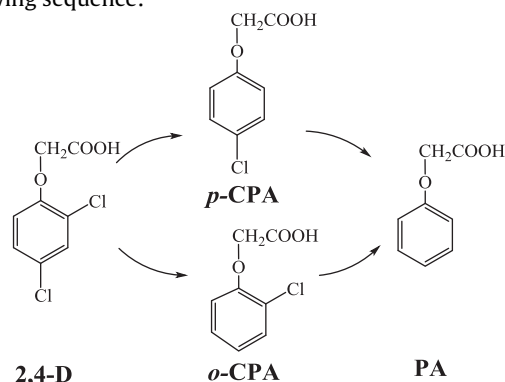
In order to investigate the electrochemical activity of the electrodes, the linear sweep voltammetry measurements of Ni, Pd/Ni and nTiN doped Pd/Ni foam electrodes were performed. As shown in Fig. 3, the hydrogen evolution reaction (HER) was enhanced when Pd was loaded onto the Ni foam surface as a cathode, meanwhile it further increased after nTiN was doped into the electrode. Electrocatalytic volcano plots are built when the catalytic activity of a material for the HER is plotted as a function of the hydrogen-metal bond strength [38]. According to electrocatalytic volcano plots, it revealed that Pd was the earlier polarized portion than Ni foam substrate that initiated the HER [39]. The electrical resistivity of nTiN was found to be $0.0022 \Omega \text{ m}$, which was lesser than that of Pd ($105.4 \Omega \text{ m}$). The good electrical conductivity of nTiN might accelerate the electron transfer inside the Pd layer, thus boosting the cathode current as compared to Pd/Ni electrode. In addition, the modification effect on the electrode surface by nTiN doping provided more polarized portion for HER. In this study, it was inappropriate to conclude the dechlorination effectiveness of the electrode based simply on the linear sweep voltammetry data. But it offered some insights about the effectiveness of the dechlorination of nTiN doped electrode. The source of hydrogen was considered to be critical for effective dechlorination treatment [37]. Sufficient molecular hydrogen source supported by HER on nTiN doped electrodes would increase the amount of $[\text{H}]$ chemisorbed on Pd, which resulted to significantly improve the dechlorination efficiency.

3.2. Comparative experiments on 2,4-D dechlorination by nTiN doped Pd/Ni and Pd/Ni foam electrodes

Dechlorination of 2,4-D by nTiN doped Pd/Ni and Pd/Ni foam electrodes was investigated under controlled experimental conditions. It was found that nTiN has a positive impact on the electrocatalytic activity of the electrodes. The concentration of 2,4-D drastically decreased from $0.226 \text{ mmol L}^{-1}$ to $0.0003 \text{ mmol L}^{-1}$ when nTiN doped electrodes were used and the 2,4-D removal efficiency reached 100% after 2 h of electrolysis (Fig. 4b), while the removal efficiency reached only 57.13% with Pd/Ni electrodes (Fig. 4a). An average current efficiency of 6.7% for 2,4-D dechlorination at 2 h was attained using nTiN doped electrodes, which nearly doubled that of Pd/Ni electrodes (3.7%). The complete dechlorination product (PA) was measured as the only final product during the two electrolyses. A comparative experiment was performed using a bare Ni foam electrode as cathode. However, no 2,4-D reduction was observed even after 4 h of the reaction (Fig. S1). It is generally known that two mechanisms have been proposed for electrocatalytic dechlorination including direct and indirect reductive dechlorination. The former is based on the theory of electron

transfer (ET) [40], whilst the latter mainly relies on the Pd catalytic performance of active atomic hydrogen $[\text{H}]$ chemisorption [41]. Our experiment result revealed that the direct mechanism was not adequate to explain 2,4-D dechlorination using Ni foam, which presumably caused by the energy barriers [20,42] and the greater reduction difficulty of 2,4-D than other COCs [43]. Therefore, the effective dechlorination of 2,4-D on Pd loaded electrodes could be better explained by the indirect mechanism. Adsorption experiment was additionally performed to investigate the sorption characteristic of 2,4-D on nTiN doped Pd/Ni electrodes without current density. However, negligible amount of absorbed 2,4-D onto the electrodes was detected after 2 h. The poor adsorptive performance of the nTiN doped Pd/Ni electrode was in accordance with the mass balance data, which was nearly 100% during 2 h reaction.

Partially dechlorinated intermediate products including *o*-CPA and *p*-CPA were detected at low levels. As shown in Fig. 4 insets, when an nTiN doped electrode used, the *o*-CPA and *p*-CPA maximum concentrations reached $6.12 \mu\text{mol L}^{-1}$ and $0.93 \mu\text{mol L}^{-1}$ at 60 min, respectively, then decreased afterwards to $0 \mu\text{mol L}^{-1}$. But in the case of Pd/Ni electrode, *o*-CPA and *p*-CPA continued to accumulate during the whole electrolysis and reached $17.0 \mu\text{mol L}^{-1}$ and $1.62 \mu\text{mol L}^{-1}$, respectively, after 2 h of the reaction. The co-existence of *o*-CPA and *p*-CPA in two cases implied that both types of electrodes dechlorinated 2,4-D in an successive reduction pathway, in which 2,4-D was first converted to *o*-CPA or *p*-CPA and then further reduced to PA. The key processes could be described in the following sequence:



Despite the existence of two different dechlorination pathways, the concentration of *o*-CPA was detected much higher than that of *p*-CPA and the intermediate products' relative concentration covered a wide range of approx. 6–11 times. In addition, *o*-CPA was detected by HPLC prior to *p*-CPA in the cathode solution. These results demonstrated that both electrodes apparently possessed much higher selectivity to *o*-CPA and the chlorine atom located at *para*-position was more susceptible to be eliminated than that at *ortho*-position, which was in agreement with reported studies [44,45]. The ease of C–Cl bond scission was reported to be depended on the instantaneous adsorption of the organic compound on Pd surface [46]. Hence, the selectivity phenomenon was mainly due to the steric hindrance of the functional group ($-\text{OCH}_2\text{COOH}$) of 2,4-D, which blocked the formation of *ortho*-Cl-metal bond at electrodes and impeded the further dechlorination process.

The pseudo-first order kinetic model was commonly used to describe pathways for dechlorination of COCs in an aqueous solution [20,34,37,47]. Previously established literature showed that this model was pervasive in the electrocatalytic dechlorination. In a system in conformity with pseudo-first order kinetic model, the reaction rate is proportional to the instantaneous contaminant concentration, which can be described as Eq. (1):

$$-\frac{dC}{dt} = k \cdot C \quad (1)$$

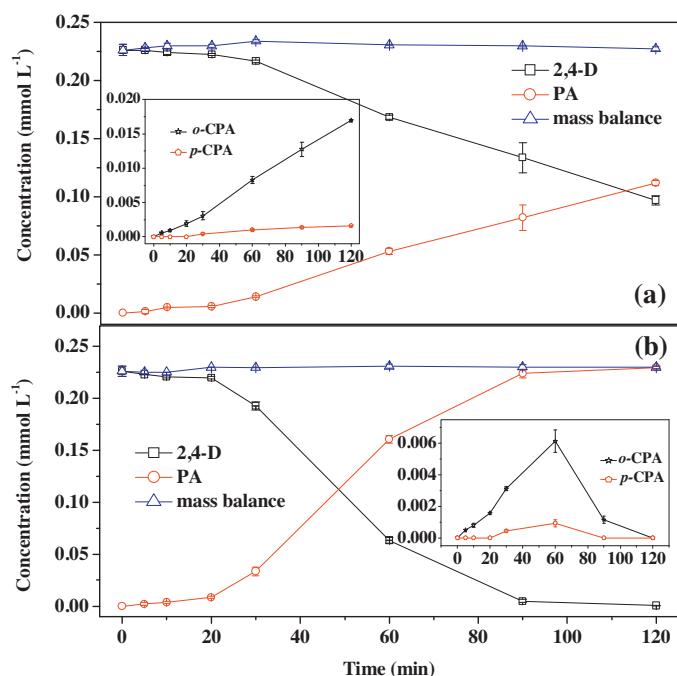


Fig. 4. Intermediates and final products of dechlorination of 2,4-D through (a) Pd/Ni foam electrode and (b) nTiN doped Pd/Ni foam electrode (applied current density = 1.667 mA cm⁻², initial concentration of 2,4-D = 50 mg L⁻¹, Na₂SO₄ = 10 mmol L⁻¹, nTiN doping content = 2 mg and Pd loading = 0.44 mg cm⁻²).

where C is contaminant concentration and k represents observed first-order rate constant. The electrocatalytic dechlorination process of COCs in aqueous solutions is a complicated system, which involves various parameters including electrode catalytic activity, current density, solution property and the contaminant concentration. However, the well application of pseudo-first order kinetic model for the previous works indicated that in a certain experiment, the COCs dechlorination rate was the function of its concentration. Unfortunately, when we used this model to describe the 2,4-D reduction by nTiN doped Pd/Ni electrodes, the correlation coefficient (R^2) value could only reach 0.86. It is obvious that the 2,4-D concentration and the dechlorination rate did not well conform to Eq. (1) for the plateau during the first 30 min of the experiments. This implied the inconformity of pseudo-first order kinetic model for the dechlorination behavior by nTiN doped Pd/Ni electrodes and at the same time suggested a more complicated mechanism for dechlorination. More details to this discussion can be seen in Section 3.4.

3.3. Effect of nTiN doping content and palladium loading on the dechlorination efficiency of 2,4-D

The optimum nTiN doping content and the impact of Pd loadings on the dechlorination efficiency was investigated. As illustrated in Fig. 5a, 72.01% 2,4-D conversion was achieved with an optimum nTiN doping content of 2 mg with a fixed Pd loading after 1 h of electrolysis. Reducing the nTiN doping content from 1 mg to 0 mg led to 2,4-D decreasing conversion from 52.94% to 25.56%. Meanwhile, the similar decline trend of electrode's catalytic performance was also observed when the nTiN doping content increased to 3 mg and 4 mg with decreasing 2,4-D conversion from 71.19% to 61.60%. Moreover, the conversion was further reduced to 54.63%, when 5 mg doping content was added. PA yield was calculated to be less than 3% below the corresponding value of 2,4-D conversion. This minor gap between 2,4-D conversion and PA yield could be attributed to the existence of intermediate products and

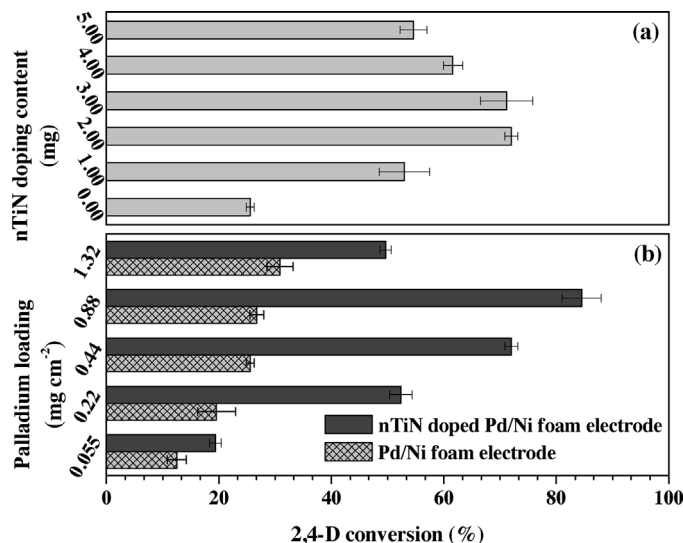


Fig. 5. Effect of nTiN doping and palladium loading on the dechlorination efficiency of 2,4-D ((a) applied current density = 1.667 mA cm⁻², initial concentration of 2,4-D = 50 mg L⁻¹, Na₂SO₄ = 10 mmol L⁻¹, reaction time = 1 h and Pd loading = 0.44 mg cm⁻²; (b) applied current density = 1.667 mA cm⁻², initial concentration of 2,4-D = 50 mg L⁻¹, Na₂SO₄ = 10 mmol L⁻¹, nTiN doping content = 2 mg and reaction time = 1 h).

indicated that the majority of 2,4-D was converted to PA. Fig. 5b demonstrated the effect of Pd loading on electrode dechlorination performance. Firstly, it showed that the dechlorination efficiency improved slightly when the Pd loading at Pd/Ni electrode increased. 2,4-D conversion improved only from 12.5% to 30.88% as the Pd loading increased from 0.055 mg cm⁻² to 1.32 mg cm⁻², which was in agreement with the previously reported results [29]. Secondly, the identical nTiN doping content had a different impact on the dechlorination efficiency at diverse Pd loadings, as shown in Fig. 5b. When the Pd loading increased from 0.055 mg cm⁻² to 0.88 mg cm⁻² the nTiN doping content (2 mg) exhibited significant influence on the dechlorination efficiency. The enhancement of 2,4-D conversion increased from 6.86% to 57.76%. Nevertheless, the enhancement of 2,4-D conversion decreased to only 18.8% when 1.32 mg cm⁻² Pd loading was employed indicating the positive impact was suppressed.

Catalytic reaction site was a critical factor during the hydrodechlorination (ECH) process. High Pd loading was recognized to favor the production of catalytically active hydrogen atom [H]. When Pd on the Ni substrates was over one layer, the additional Pd would be generated by overlapping the existing catalytic reaction sites first and inevitably consumed the available sites for Pd–Cl bond formation. As a result, minor improvement of dechlorination efficiency was achieved by Pd/Ni electrodes as the Pd loading increased.

The exciting positive impact of nTiN on the dechlorination efficiency could be manifested in three aspects. Firstly, Thotiyl et al. [35] reported the difference of electronic nature between Pd–nTiN interface with either Pd or nTiN, which was also demonstrated in our XPS analysis. The interaction possibly created an electron deficiency on Pd particles, which increased the probability of 2,4-D instant adsorption on the electrode surface by Pd–Cl bond. Secondly, nTiN had been used for effective debromination [33], which showed the catalytic characteristic of nTiN by generating the active hydrogen atom [H]. In this study, the co-existence of Pd with nTiN further facilitated the HER process on the electrodes, which provided more chemisorbed hydrogen atom by intercalating hydrogen within Pd lattices. Thirdly, the geometric effect was recognized to have a significant impact on the catalyst performance [48]. The

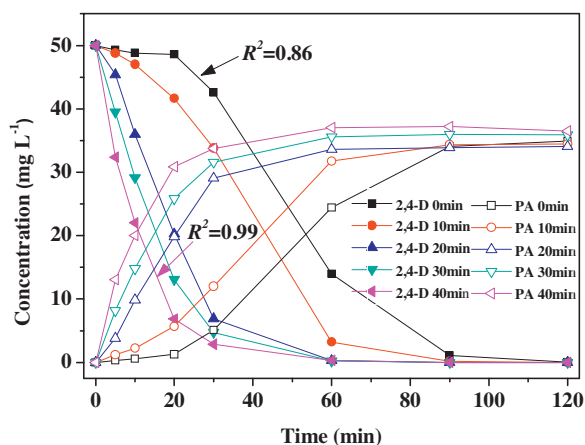


Fig. 6. Effect of pre-treatment time on the removal efficiency of 2,4-D (applied current density = 1.667 mA cm^{-2} , initial concentration of 2,4-D = 50 mg L^{-1} , $\text{Na}_2\text{SO}_4 = 10 \text{ mmol L}^{-1}$, nTiN doping content = 2 mg , Pd loading = 0.44 mg cm^{-2} and pre-treatment applied current density = 1.667 mA cm^{-2}).

modification effect of nTiN on Pd layer was also confirmed from our FE-SEM study. The upper flaky wrinkle structure of the Pd layer served with more specific surface area and created more active sites for catalytic dechlorination. Further addition of nTiN beyond the optimum doping content presented more difficulty to form flaky wrinkle structures. The nTiN aggregated and covered the available Pd active sites that eventually prevented them from contacting with reactants. It should be pointed out that when the nTiN doping content increased beyond 5 mg , there was certain amount of nTiN still remained in solution after 12 h of shaking during the electroless electrode preparation process. High nTiN solution concentration made the Ni foam heavily covered by nTiN that inhibited the replacement reaction with Pd^{2+} . Thus, it revealed that the electroless preparation of nTiN doping content was limited by the maximum doping content. This problem needs to be further investigated and could delve further into an important research topic for future studies. When 1.32 mg cm^{-2} Pd loading was applied, a decline in the dechlorination efficiency was found to appear for nTiN doped electrodes, most likely resulting from the insufficient amount of nTiN to achieve the considerable positive modification of the Pd layer.

3.4. Proposed adsorption theory for palladium chemisorbing active hydrogen atom [H]

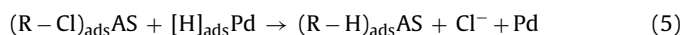
We reported in Section 3.2 that a plateau of 2,4-D dechlorination occurred at the first quarter in 2 h reaction time. Tsyganok et al. [49] also observed such a plateau toward the middle of a 4 h long reaction when they employed a Pd-loaded carbon felt electrode to dechlorinate 2,4-D. However, no other published literature reported this phenomenon yet. In order to further investigate this phenomenon, a series of experiments were performed, as elaborated below.

The effect of pre-treatment time on the removal efficiency of 2,4-D using nTiN doped Pd/Ni electrodes was investigated. In our study, pre-treatment involved the electrolysis of nTiN doped Pd/Ni electrodes in a 10 mmol L^{-1} Na_2SO_4 aqueous solution without 2,4-D in the cathode cell. After a period of predetermined time set, 2,4-D was immediately introduced into the cathode cell for dechlorination. It should be pointed out that during this experiment series, the electrode was not pulled out from the cathode solution for any further treatment. When the pre-treatment time was extended, the plateau disappeared gradually, as shown in Fig. 6. The correlation coefficient (R^2) of a pseudo-first order kinetic model for

these five experiments with a pre-treatment time of 0, 10, 20, 30 and 40 min were calculated to be 0.86, 0.87, 0.95, 0.98 and 0.99, respectively. Thus, it indicated that the pseudo-first order kinetic model fit better with 2,4-D dechlorination by nTiN doped Pd/Ni electrodes when the pre-treatment time increased. Tsyganok et al. [49] ascribed the effects of pre-treatment of the electrode to (i) the change in spatial distribution of the supported Pd clusters and (ii) the formation of hydrogen-saturated Pd phase. In order to verify analysis (i), two control experiments were conducted. In the first control experiment, after 30 min pre-treatment, the nTiN doped Pd/Ni electrode was taken out from the solution and washed with deionized water for several times. Meanwhile, the solution inside the cathode and anode cell was replaced to exclude any possible alteration in each cell. No significant changes were observed during the dechlorination and the plateau still remained after the aforementioned treatment period (Fig. S2). It revealed that the morphological changes appeared on the electrode during the pre-treatment did not have any effect on the dechlorination in our case. The second control experiment was performed to verify the inadequacy of analysis (i) in the view of nTiN doped Pd/Ni electrode stability. It revealed that even after 20 successive dechlorination cycles, nearly 100% of 2,4-D dechlorination was achieved after 2 h (Fig. S3). No obvious decline trend in dechlorination efficiency of the electrodes was observed during the consecutive experiments indicating of excellent electrode stability. From a practical point of view, nTiN doped Pd/Ni electrodes could be selected as promising electrodes because of their excellent robustness in environmental applications.

The chamber cell solution pH was detected during the experiments using nTiN doped Pd/Ni electrode with and without pre-treatment. Without the pre-treatment, the initial pH was recorded to be about 3.85 due to the acidic nature of 2,4-D. pH drastically increased to 10.13 in the first 10 min, then raised gradually to 11.08 during the rest of the reaction time. In the case of 30 min pre-treatment experiment, the initial solution pH increased from 7.08 to 10.88 during the same pre-treatment time. The pH decreased a little to 10.74 after adding 2,4-D. Moreover, as the dechlorination reaction proceeded, the final pH reached 11.21 (Fig. S4). In order to investigate any possible effect in the variations of initial pH on the formation of the plateau, an experiment was performed with the initial pH of 10.74. Minor variation was recorded in the dechlorination efficiency (Fig. S5). It was probable that most stages of the experiment proceeded between pH 10–11 and the dechlorination efficiency remained stable in such a narrow pH range [29,37].

Analysis (ii) had never been verified through experiments by other researchers so far. In our work, for the first time, it was extensively investigated. For this purpose, after certain pre-treatment time periods the current was quickly interrupted, meanwhile 2,4-D was added directly into the cathode cell solution for further reaction without current density. Consequently, interesting results were obtained in this confirmatory experiment. As illustrated in Fig. 7a, 2,4-D was immediately dechlorinated within the initial 5 min. The formation of the resulting product (PA) could be seen as the 2,4-D concentration declined. Moreover, the intermediate products (CPA) were also detected as shown in Fig. 8b. In the absence of current density, the stored active hydrogen atom [H] in Pd was postulated to play a leading role in the dechlorination of 2,4-D. The widely known indirect reduction mechanism may involve the following pathways, as written in Eqs. (2)–(6):



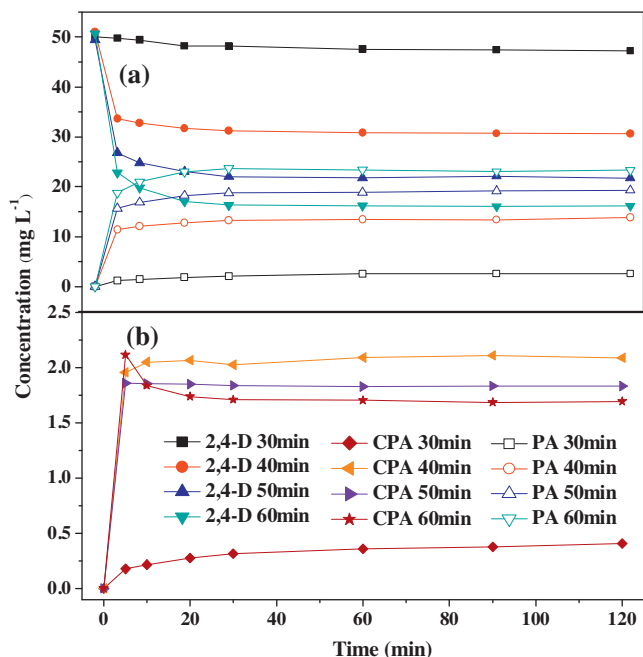


Fig. 7. Effect of pre-treatment time on the catalytic dechlorination efficiency of 2,4-D without current density (initial concentration of 2,4-D = 50 mg L⁻¹, Na₂SO₄ = 10 mmol L⁻¹, nTiN doping content = 2 mg, Pd loading = 0.44 mg cm⁻² and pre-treatment applied current density = 1.667 mA cm⁻²).



where AS represents the active sites for reactant adsorption and [H]_{ads} is the chemisorbed active hydrogen atom. According to the pathway, the amount of [H] consumed for generating per one molecule of CPA and PA was 1 and 2, respectively. Therefore, the total hydrogen atom consumed for dechlorination at each time interval could be calculated according to Eq. (7):

$$N_{[H]} = (2 \times M_{PA} + M_{o-CPA} + M_{p-CPA}) \times V_{Cs} \quad (7)$$

where $N_{[H]}$ (mmol) is the number of moles of active hydrogen atom [H] consumed for dechlorination. M_{PA} , M_{o-CPA} and M_{p-CPA} (mmol L⁻¹) are the molar concentration of PA, o-CPA and p-CPA in mM, respectively, existed in the cathode solution. V_{Cs} represents the volume of the cathode solution. The result revealed that [H] consumed gradually in the process with higher consumption rate at the beginning (Fig. 8a). This proved that [H] did not disappear

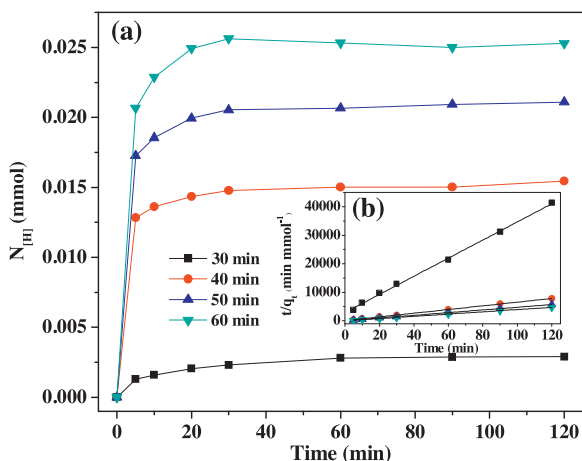


Fig. 8. Total consumed active hydrogen atom [H] for 2,4-D dechlorination (a) and pseudo second-order kinetic plots (b).

instantly once the current density was interrupted. Moreover, with the increased pre-treatment time, more [H] was available for the dechlorination. The curves of 2,4-D dechlorination without current density varied significantly from that with current density indicating that the absence of subsequent [H] by water electrolysis inhibited the continuity of 2,4-D dechlorination after the first 5 min. Therefore, the continuous supply of available [H] was the rate-determining step for dechlorination.

It should be noted that in absence of current density experiment with 30 min pre-treatment, the dechlorination efficiency of 2,4-D was too low as compared to those in other three experiments. Meanwhile, the amount of dechlorination consumed [H] was also low only in this particular experiment. It seemed that [H] experienced an explosive growth after 30 min, which was in accordance with the 30 min plateau. This was not a coincidence and there must be something “capturing” the [H]. Based on the aforementioned analysis, an adsorption theory for Pd chemisorbing active hydrogen atom [H] was proposed. The theory held that there existed an equilibrium between adsorption and desorption of [H] inside the Pd layer. The desorbed [H] was used for either dechlorination or HER via Tafel and Heyrovsky steps [41]. According to metal hydrogen storage mechanism [50,51], H₂ was first adsorbed on the metal surface and then affected by metal atoms by dissociating H₂ into two [H]. Afterward, [H] entered into the metal lattice, occupied the inter-space around metal atom and formed hydrogen solid solution phase (MH_x). MH_x would reversibly react with molecular hydrogen to form metal hydride phase (MH_y), which had different properties from hydrogen solid solution due to the participation of chemical reaction. The reversible reaction could be described as Eq. (8):



As a result, the forms of hydrogen on Pd experienced two phases including hydrogen in solid solution phase and hydrogen in metal hydride phase, among which only hydrogen in the first phase was active and supposed to be utilized for dechlorination. The simultaneous presence of spillover hydrogen, chemisorbed hydrogen and hydrides in the Pd-doped substrate had also been demonstrated in literature [52]. Fig. 8a illustrates that [H] for dechlorination was released quickly in the initial 5 min. Afterward, the releasing rate was found to reduce a lot. These two stages were an obvious evidence of the existence of two different phases, which led to the different [H] releasing rates. This theory could be used to well explain the plateau occurred during the first 30 min of the dechlorination by nTiN doped Pd/Ni electrodes. The [H] in hydrogen solid solution was mainly consumed to reach an equilibrium other than dechlorinating 2,4-D in the first 30 min. After reaching equilibrium, surplus [H] was utilized for dechlorination or HER process. We speculated two reasons for the seldom observation of the plateau in other studies. One could be the long time interval from beginning to the first sampling and that might cause the loss of some specific details. The other one could be the co-existence of direct and indirect mechanisms, which led to the disappearance of the plateau in the beginning of the electrolysis period [20,37]. The electron transfer would supplement the lack of [H] in the preliminary stage of the electrolysis.

Pseudo second-order adsorption model was usually used for the adsorption on solid, which can be written as Eq. (9):

$$\frac{t}{q_t} = \frac{1}{k \cdot q_e^2} + \frac{t}{q_e} \quad (9)$$

where q_t and q_e represent the amounts of desorbed [H] used for the dechlorination at any time t or at equilibrium time (mmol), k is the second-order rate constant of desorption (mmol⁻¹ min⁻¹). The values of k and q_e can be extrapolated from the slope and intercept by plotting t/q_t against t .

Table 1

Pseudo second-order desorption kinetics constant for total consumed active hydrogen atom [H] desorbed from Pd (initial concentration of 2,4-D = 50 mg L⁻¹, Na₂SO₄ = 10 mmol L⁻¹, nTiN doping content = 2 mg, Pd loading = 0.44 mg cm⁻², and pre-treatment applied current density = 1.667 mA cm⁻²).

Parameter	Pre-treatment time (min)			
	30	40	50	60
k (mmol ⁻¹ min ⁻¹)	34.622	43.331	34.839	63.814
q_e (mmol)	0.0032	0.0155	0.0212	0.0253
R^2	0.9987	0.9997	1	0.9998

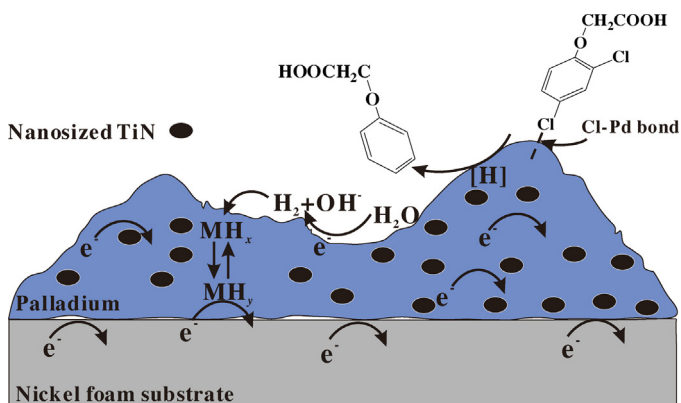


Fig. 9. Schematic illustration of 2,4-D dechlorination mechanism by nTiN doped Pd/Ni electrode.

This model was applied to describe the [H] adsorption behavior on Pd. As shown in Fig. 8b, the pseudo second-order adsorption model fit well with the experimental data ($R^2 > 0.99$). The linearity indicated that this model could be applied perfectly. To a certain degree, the hydrogen adsorption process in the Pd layer was similar to the ordinary adsorption process in nature. The parameters obtained by linear regression analysis are listed in Table 1 demonstrating that [H] in hydrogen solid solution for 2,4-D dechlorination increased as the pre-treatment time increased as well as the rate constant also showed a rising trend.

3.5. 2,4-D dechlorination mechanism by nTiN doped Pd/Ni electrode

On the basis of the experiments performed and the analysis presented earlier, it could be hypothesized that an indirect mechanism using nTiN doped Pd/Ni electrode was mainly involved for 2,4-D dechlorination. As illustrated in Fig. 9, H₂ was first produced by water electrolysis in the cathode cell, followed by that the generation of active hydrogen atoms [H] to enhance the catalytic efficiency of 2,4-D dechlorination. But there existed equilibrium between the hydrogen atoms in the solid solution phase and those in the metal hydride phase. During the dechlorination, weak Pd–Cl bonds were formed on the Pd particles and subsequently followed to be attracted by [H] in hydrogen solid solution. After the C–Cl scission, the product was desorbed into the solution, regenerating active sites on Pd. In order to better describe the dechlorination pathway, Eq. (3) could be modified to become Eq. (10), which could be written as follows:



4. Conclusion

In summary, nTiN doped Pd/Ni foam electrodes were successfully synthesized via electroless deposition method. The

as-prepared electrodes were systematically characterized by a variety of techniques including FE-SEM, TEM, XPS, XRD and LSV. FE-SEM images demonstrated that there existed two different morphologies in deposited Pd after nTiN doping. The novel electrode showed excellent stability and higher catalytic properties than normal Pd/Ni foam electrodes for 2,4-D dechlorination, which achieved nearly 72.01% removal efficiency of 2,4-D (0.226 mmol L⁻¹) within 1 h with the optimal nTiN doping content of 2 mg when Pd loading was 0.44 mg cm⁻². However, increasing or decreasing the nTiN doping content there were a declined trend in 2,4-D removal efficiency and only 54.63% and 25.56% attenuations were achieved with the nTiN doping content of 5 mg and 0 mg, respectively, after 1 h of the reaction. The identical nTiN doping content (2 mg) had different impacts on the dechlorination efficiency at various Pd loadings. Improvement in 2,4-D removal efficiency from 6.86% to 57.76% with an increased palladium loadings from 0.055 mg cm⁻² to 0.88 mg cm⁻² was achieved after 1 h, but it reduced to only 18.8% when the Pd loading increased to 1.32 mg cm⁻². Cathodic polarization was found to inhibit the electrode's catalytic deactivation process as a result of the oxidation and/or chloride adsorption. Successive 2,4-D reduction process was observed and *o*-CPA, *p*-CPA and PA were detected as the only transformation products. Application of nTiN was found to improve the catalytic ability of the electrode in three aspects, namely electronic nature, HER process and geometric effect. Moreover, an adsorption mechanism for Pd chemisorption [H] was proposed, which explained that the forms of hydrogen on Pd experienced two phases and the existence of equilibrium between active phase (hydrogen in solid solution phase) and insert phase (hydrogen in metal hydride phase). The indirect reduction mechanism of the 2,4-D dechlorination on the electrode showed that the active hydrogen atoms [H] was the main impetus for effective 2,4-D dechlorination on nTiN doped Pd/Ni foam electrodes.

Acknowledgements

The authors acknowledge financial support from the National Natural Science Foundation (No. 21277119) and the Science and Technology Project of Zhejiang Province, China (No. 2012C23061).

Appendix A. Supplementary data

Supplementary data associated with this article can be found, in the online version, at <http://dx.doi.org/10.1016/j.apcatb.2014.04.004>.

References

- [1] A. Boivin, S. Amellal, M. Schiavon, M.T. van Genuchten, *Environ. Pollut.* 138 (2005) 92–99.
- [2] J.M. Salman, B.H. Hameed, *Desalination* 256 (2010) 129–135.
- [3] C. Badellino, C.A. Rodrigues, R. Bertazzoli, *J. Hazard. Mater.* 137 (2006) 856–864.
- [4] K. Zhu, C. Sun, H. Chen, S.A. Baig, T. Sheng, X. Xu, *Chem. Eng. J.* 223 (2013) 192–199.
- [5] K. Shareef, G. Shaw, *Chemosphere* 72 (2008) 8–15.
- [6] Y. Yasman, V. Bulatov, V.V. Gridin, S. Agur, N. Galil, R. Armon, I. Schechter, *Ultrason. Sonochem.* 11 (2004) 365–372.
- [7] S. Cenkci, M. Yildiz, I.H. Cigerci, A. Bozdağ, H. Terzi, E.S.A. Terzi, *Ecotoxicol. Environ. Safety* 73 (2010) 1558–1564.
- [8] J.S. Bus, L.E. Hammond, *Crop. Prot.* 26 (2007) 266–269.
- [9] B.H. Hameed, J.M. Salman, A.L. Ahmad, J. Hazard. Mater. 163 (2009) 121–126.
- [10] G. Chen, Z. Wang, D. Xia, *Electrochem. Commun.* 6 (2004) 268–272.
- [11] C.B. Wang, W.X. Zhang, *Environ. Sci. Technol.* 31 (1997) 2154–2156.
- [12] X. Lv, G. Jiang, X. Xue, D. Wu, T. Sheng, C. Sun, X. Xu, *J. Hazard. Mater.* 262 (2013) 748–758.
- [13] H. Dong, I.M.C. Lo, *Water Res.* 47 (2013) 2489–2496.
- [14] D.L. Freedman, J.M. Gossett, *Appl. Environ. Microb.* 55 (1989) 2144–2151.
- [15] K.R. Sowers, H.D. May, *Curr. Opin. Biotechnol.* 24 (2013) 482–488.
- [16] R.B. Payne, H.D. May, K.R. Sowers, *Environ. Sci. Technol.* 45 (2011) 8772–8779.
- [17] S.K. Fagervold, J.E.M. Watts, H.D. May, K.R. Sowers, *Water Res.* 45 (2011) 3899–3907.

- [18] Z. Sun, X. Wei, X. Hu, K. Wang, H. Shen, *Colloid Surf. A* 414 (2012) 314–319.
- [19] B. Yang, G. Yu, X. Liu, *Electrochim. Acta* 52 (2006) 1075–1081.
- [20] W. Xie, S. Yuan, X. Mao, W. Hu, P. Liao, M. Tong, A.N. Alshawabkeh, *Water Res.* 47 (2013) 3573–3582.
- [21] C. Comninellis, G. Chen, *Electrochemistry for the Environment*, Springer, New York, 2010.
- [22] A.I. Tsyganok, K. Otsuka, *Electrochim. Acta* 43 (1998) 2589–2596.
- [23] J. Simonet, *Electrochem. Commun.* 7 (2005) 619–626.
- [24] J. Li, H. Liu, X. Cheng, Y. Xin, W. Xu, Z. Ma, J. Ma, N. Ren, Q. Li, *Ind. Eng. Chem. Res.* 51 (2012) 15557–15563.
- [25] Y. Gao, S. Chen, D. Cao, G. Wang, J. Yin, *J. Power Sources* 195 (2010) 1757–1760.
- [26] W. Yang, S. Yang, W. Sun, G. Sun, Q. Xin, *Electrochim. Acta* 52 (2006) 9–14.
- [27] X.H. Huang, J.P. Tu, X.H. Xia, X.L. Wang, J.Y. Xiang, *Electrochem. Commun.* 10 (2008) 1288–1290.
- [28] I.F. Cheng, Q. Fernando, N. Korte, *Environ. Sci. Technol.* 31 (1997) 1074–1078.
- [29] Z. He, J. Sun, J. Wei, Q. Wang, C. Huang, J. Chen, S. Song, *J. Hazard. Mater.* 250–251 (2013) 181–189.
- [30] R. Aghababazadeh, A.R. Mirhabibi, B. Rand, S. Banijamali, J. Pourasad, M. Gha-hari, *Surf. Sci.* 601 (2007) 2881–2885.
- [31] S. Kawano, J. Takahashi, S. Shimada, *J. Am. Ceram. Soc.* 86 (2003) 1609–1611.
- [32] G.R. Li, F. Wang, Q.W. Jiang, X.P. Gao, P.W. Shen, *Angew. Chem. Int. Edit.* 49 (2010) 3653–3656.
- [33] J.Y. Su, N. Lu, J.J. Zhao, H.T. Yu, H. Huang, X.L. Dong, X. Quan, *J. Hazard. Mater.* 231 (2012) 105–113.
- [34] K. Zhu, S.A. Baig, J. Xu, T. Sheng, X. Xu, *Electrochim. Acta* 69 (2012) 389–396.
- [35] M.M.O. Thotiyil, T.R. Kumar, S. Sampath, *J. Phys. Chem. C* 114 (2010) 17934–17941.
- [36] I.G. Casella, M. Contursi, *J. Electroanal. Chem.* 692 (2013) 80–86.
- [37] A. Li, X. Zhao, Y. Hou, H. Liu, L. Wu, J. Qu, *Appl. Catal. B: Environ.* 111 (2012) 628–635.
- [38] J. Greeley, T.F. Jaramillo, J. Bonde, I.B. Chorkendorff, J.K. Nørskov, *Nat. Mater.* 5 (2006) 909–913.
- [39] B. Yang, G. Yu, J. Huang, *Environ. Sci. Technol.* 41 (2007) 7503–7508.
- [40] C. Costentin, M. Robert, J.M. Savéant, *Chem. Phys.* 324 (2006) 40–56.
- [41] Z. Sun, X. Wei, Y. Han, S. Tong, X. Hu, *J. Hazard. Mater.* 244–245 (2012) 287–294.
- [42] T. Li, J. Farrell, *Environ. Sci. Technol.* 34 (2000) 173–179.
- [43] C.A. Ma, H. Ma, Y.H. Xu, Y.Q. Chu, F.M. Zhao, *Electrochem. Commun.* 11 (2009) 2133–2136.
- [44] H. Zhou, J. Han, S.A. Baig, X. Xu, *J. Hazard. Mater.* 198 (2011) 7–12.
- [45] A.I. Tsyganok, K. Otsuka, *Appl. Catal. B: Environ.* 22 (1999) 15–26.
- [46] K. Mackenzie, H. Frenzel, F.D. Kopinke, *Appl. Catal. B: Environ.* 63 (2006) 161–167.
- [47] Z. He, K. Lin, J. Sun, L. Wen, C. Gao, J. Chen, S. Song, Y. Qian, W. Liu, *Electrochim. Acta* 109 (2013) 502–511.
- [48] B. Coq, F. Figueras, *J. Mol. Catal. A: Chem.* 173 (2001) 117–134.
- [49] A.I. Tsyganok, I. Yamanaka, K. Otsuka, *J. Electrochem. Soc.* 145 (1998) 3844–3850.
- [50] L.L. Jewell, B.H. Davis, *Appl. Catal. A: Gen.* 310 (2006) 1–15.
- [51] M. Latroche, *J. Phys. Chem. Solids* 65 (2004) 517–522.
- [52] C. Amorim, M.A. Keane, *J. Colloid Interf. Sci.* 322 (2008) 196–208.